Hydrogenase biomimetics with redox-active ligands: Electrocatalytic proton reduction by $[Fe_2(CO)_4(\kappa^2\text{-diamine})(\mu\text{-edt})]$ (diamine = 2,2′-bipy, 1,10-phen)

Shishir Ghosh,[a,b,e,*] Ahibur Rahaman,[b,c] Katherine B. Holt,[a] Ebbe Nordlander,[c] Michael G. Richmond,[d] Shariff E. Kabir[b] and Graeme Hogarth[a,e,*]

[a]*Department of Chemistry, University College London, 20 Gordon Street, London WC1H OAJ, UK*

[b]*Department of Chemistry, Jahangirnagar University, Savar, Dhaka 1342, Bangladesh: Email: sghosh_006@yahoo.com*

[c]*Inorganic Chemistry Research Group, Chemical Physics, Center for Chemistry and Chemical Engineering, Lund University, Box 124, SE-221 00 Lund, Sweden*

[d]*Department of Chemistry, University of North Texas, Denton, TX 76209, USA*

[e]*Department of Chemistry, King's College London, Britannia House, 7 Trinity Street, London SE1 1DB, UK: Email: graeme.hogarth@kcl.ac.uk*

Abstract

Diiron complexes bearing redox active diamine ligands have been studied as models of the active site of [FeFe]-hydrogenases. Heating $[Fe_2(CO)_6(\mu\text{-edt})]$ (edt = 1,2-ethanedithiolate) with 2,2′-bipyridine (2,2′-bipy) or 1,10-phenanthroline (1,10-phen) in MeCN in the presence of Me_3NO leads to the formation of $[Fe_2(CO)_4(\kappa^2\text{-2,2′-bipy})(\mu\text{-edt})]$ (**1-edt**) and $[Fe_2(CO)_4(\kappa^2\text{-1,10-phen})(\mu\text{-edt})]$ (**2-edt**), respectively, in moderate yields. In the solid-state the diamine resides in dibasal sites, while both dibasal and apical-basal isomers are present in solution. Both stereoisomers protonate readily upon addition of strong acids. Cyclic voltammetry in MeCN shows that both complexes undergo irreversible oxidation and reduction, proposed to be a one- and two-electron process, respectively. The structures of neutral **2-edt** and its corresponding one- and two-electron reduced species have been investigated by DFT calculations. In **2-edt**$^-$ the added electron occupies a predominantly ligand-based orbital, and the iron-iron bond is maintained, being only slightly elongated. Addition of the second electron affords an open-shell triplet dianion where the second electron populates an Fe-Fe σ^* antibonding orbital, resulting in effective scission of the iron-iron bond. The triplet state lies 4.2 kcal mol^{-1} lower in energy than the closed-shell singlet dianion whose HOMO correlates nicely with the LUMO of the neutral species **2-edt**.

Electrocatalytic proton reduction by both complexes has been studied in MeCN using CF_3CO_2H as the proton source. These catalysis studies reveal that while at high acid concentrations the active catalytic species is $[Fe_2(CO)_4(\mu\text{-H})(\kappa^2\text{-diamine})(\mu\text{-edt})]^+$, at low acid concentrations the two complexes follow different catalytic mechanisms being associated with differences in their relative rates of protonation.

Keywords: hydrogenase, biomimic, redox active ligand, diiron, electrochemistry, diamine

Introduction

A recent focus in the synthesis of diiron biomimetics of the active site of [FeFe]-hydrogenases centres on the incorporation of redox-active ligands[1-11] to the diiron centre such that communication between the two electrochemically active centres can be assessed,[1-3] since such communication between the diiron and tetrairon sites in the so-called *H-cluster*[2,12-15] controls the activity of the enzyme. In 2005, Pickett and co-workers reported a model complex, $[Fe_4S_4(L)_3\{Fe_2(CH_3C(CH_2S)_3)(CO)_5\}]^{2-}$ {L = 1,3,5-tris(4,6-dimethyl-3-mercaptophenyl-thio)-2,4,6-tris(*p*-tolyl-thio)benzene}, in which the entire iron-sulfur framework of the active site of iron-only hydrogenase is assembled.[2] The {4Fe4S} site in this model catalyst is easier to reduce than the {2Fe3S} site, which can transfer the added electron to the latter site.[2] Reduction of the anchored cubane from $\{4Fe4S\}^{2+}$ to $\{4Fe4S\}^{+}$ has recently been achieved in the natural system, [16a-b] and the neighbouring {4Fe4S} relay [16c] and spectroscopic and theoretical studies have suggested that such electron transfer occurs during turnover in natural systems.[2,14,15] Pickett's model catalyst can reduce protons at low over-potentials, but its inherent frailty and structural intricacy makes it practically unfeasible.

Simple non-innocent redox-active ligands have attracted much attention in recent years as surrogates for the anchored cubane cluster.[1,4,8-11,17] In this context, we have synthesized diiron biomimetics containing the redox-active diamines, 2,2′-bipyridine (2,2′-bipy) and 1,10-phenanthroline (1,10-phen), ligands capable of coordinating to metals in a wide variety of oxidation states.[18-20] Thus, 2,2′-bipy can be doubly reduced and both the π-radical mono-anion $(2,2'\text{-bipy})^{\cdot-}$ and the diamagnetic dianion $(2,2'\text{-bipy})^{2-}$ have been crystallographically characterised. [21-24] Consequently, 2,2′-bipy is able to support metals from across the periodic

table[25-31] and its complexes have numerous applications[18,19,32-46]. For example, [Ru(2,2′-bipy)$_3$]$^{2+}$ is the most widely studied one-electron photo-redox catalyst and has facilitated significant advances in energy storage, hydrogen and oxygen evolution from water and methane production from carbon dioxide.[18,19,32-35] Furthermore, the iron complex [Fe(1,10-phen)$_3$]$^{3+}$ is widely used as a coordinatively saturated, one-electron oxidant, a redox indicator, and in model compounds of biologically active substances.[36-46]

In 2007, Schollhammer and co-workers reported the first example of a [FeFe]-biomimetic diiron complex containing a chelating diamine, namely [Fe$_2$(CO)$_4$(κ^2-1,10-phen)(μ-pdt)] (**2-pdt**) (pdt = $SCH_2CH_2CH_2S$) (Chart 1).[10] Subsequent work showed that this complex protonated upon addition of $HBF_4{\cdot}Et_2O$ to afford the bridging hydride, [Fe$_2$(CO)$_4$(κ^2-1,10-phen)(μ-H)(μ-pdt)][BF_4], which displayed poor thermal stability.[8] In contrast, the related azadithiolate complex, [Fe$_2$(CO)$_4$(κ^2-1,10-phen)(μ-adt)] (**2-adt**) (adt = $SCH_2N^iPrCH_2S$), undergoes protonation exclusively at the bridgehead nitrogen.[9] More recently, Jones and co-workers have reported a detailed study of the related 2,2′-bipyridine complex, [Fe$_2$(CO)$_4$(κ^2-2,2′-bipy)(μ-pdt)] (**1-pdt**),[11] which also protonates slowly at the metal-metal bond upon addition of strong acids. The electrochemistry of the latter was probed, the reductive chemistry being interpreted in terms of two closely spaced one-electron processes associated with the diiron centre and the 2,2′-bipy ligand.

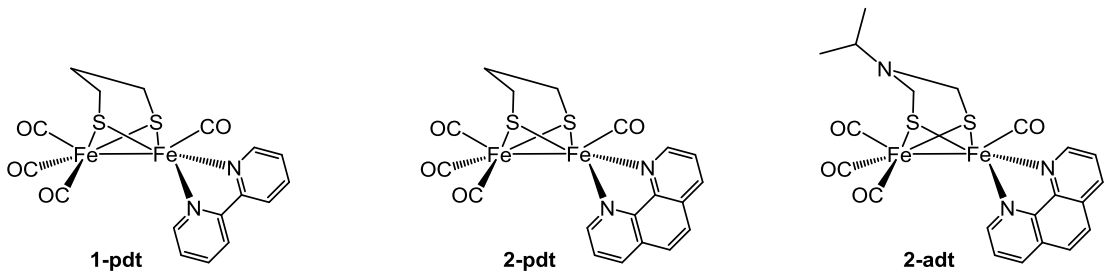

Chart 1. Biomimetic models of [FeFe]-hydrogenase containing diamine ligand.

The nature of the dithiolate backbone has a subtle but significant impact on the reductive behaviour of [Fe$_2$(CO)$_6$(μ-dithiolate)] complexes, as evidenced by the variety of products that result from the transfer of one and two electrons into such compounds,[47-56] and the dithiolate bridge exerts significant influence on the electrocatalytic pathway.[8,9,11] We therefore prepared [Fe$_2$(CO)$_4$(κ^2-2,2′-bipy)(μ-edt)] (**1-edt**) and [Fe$_2$(CO)$_4$(κ^2-1,10-phen)(μ-edt)] (**2-edt**) in order to

compare their electrochemical properties and catalytic activities towards proton reduction with the analogous pdt complexes. The results of these studies are reported herein.

Results and discussion

Synthesis and characterisation

The 2,2′-bipy complex $[Fe_2(CO)_4(\kappa^2\text{-}2,2'\text{-bipy})(\mu\text{-edt})]$ (**1-edt**) was prepared by boiling an MeCN solution of $[Fe_2(CO)_6(\mu\text{-edt})]$ with a slight excess of 2,2′-bipy in the presence of $Me_3NO{\cdot}2H_2O$, being isolated after work-up as a dark green solid in 44% yield. In a similar manner, the 1,10-phen complex, $[Fe_2(CO)_4(\kappa^2\text{-}1,10\text{-phen})(\mu\text{-edt})]$ (**2-edt**), was prepared as a green solid in 32% yield (Scheme 1). Both products are stable in the solid-state and in solution under an inert atmosphere, but solutions slowly decompose over a few hours when left standing in the air.

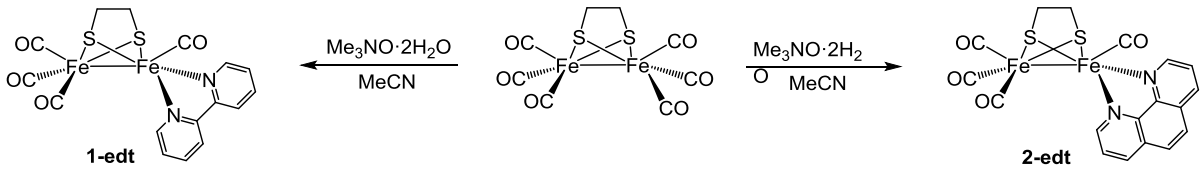

Scheme 1. Syntheses of $[Fe_2(CO)_4(\kappa^2\text{-}2,2'\text{-bipy})(\mu\text{-edt})]$ (**1-edt**) and $[Fe_2(CO)_4(\kappa^2\text{-}1,10\text{-phen})(\mu\text{-edt})]$ (**2-edt**).·

The two complexes were characterized by single crystal X-ray crystallography, the results of which are summarised in Fig. 1 and Table 1. The crystallographic analysis of **1-edt** was straightforward, and the structure consists of a single molecule that contains a plane of symmetry incorporating the heavy atoms of the edt bridge and bisecting the iron-iron vector. For **2-edt**, there are four independent molecules in the asymmetric unit with only minor differences being noted between the crystallographically independent molecules (Table 1). For each structure, the data were of a sufficiently good quality to enable location of all hydrogen atoms from difference maps, and these were refined isotropically. The two molecular structures are similar, the diamine binding in a chelating fashion and in a dibasal manner.[9-11] The Fe–Fe, Fe–S and Fe–N bond distances are unexceptional and do not differ significantly between the two, and are also quite similar to those found in **1-pdt** [11] and **2-pdt** [10]. A significant difference between the edt and pdt complexes is seen in the Fe–Fe–N bond

angles, with those in the 1,10-phen complexes being approximately 5° larger than in the pdt complexes, a difference attributed to the more sterically demanding nature of the pdt ligand. The central carbon-carbon bond of the 2,2′-bipy ligand in **1-edt** [1.464(3) Å] suggests that it is acting as a neutral diamagnetic ligand rather than a π-radical monoanion, the latter being associated with shorter carbon-carbon bonds (between 1.41 – 1.43 Å).[55,56]

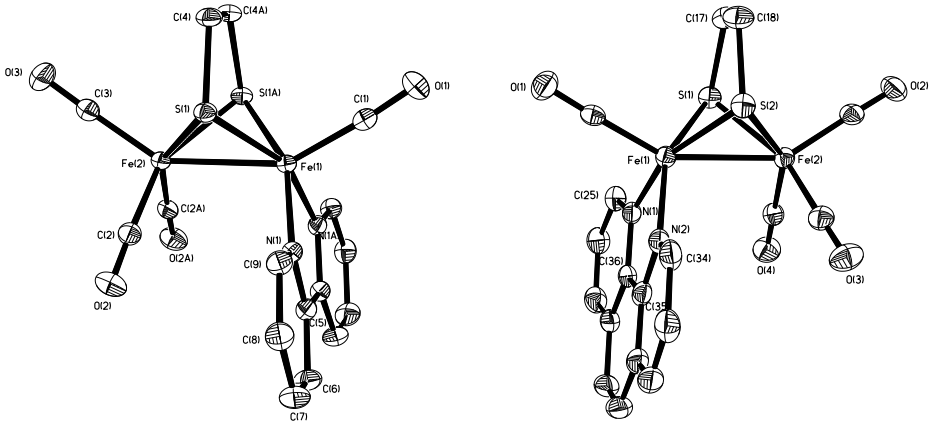

Fig. 1. ORTEP plots (50% thermal ellipsoids) of $[Fe_2(CO)_4(\kappa^2\text{-}2,2'\text{-bipy})(\mu\text{-edt})]$ (**1-edt**) and one of the four independent molecules in the asymmetric unit of $[Fe_2(CO)_4(\kappa^2\text{-}1,10\text{-phen})(\mu\text{-edt})]$ (**2-edt**). Hydrogen atoms have been omitted for clarity.

While a single isomer is seen in the solid state for both X-ray diffraction structures, two isomers are observed in solution in each case. For **2-edt**, the aromatic region of the ^{1}H NMR spectrum shows the presence of a small amount of a second isomer in a *ca*. 30:1 ratio. We suggest that the second isomer is the apical-basal isomer (as shown in Chart 2 for **1-edt**). In the case of **1-edt**, the ratio of the two isomers in CD_2Cl_2 at 298 K is *ca.* 3.5:1. Some of the aromatic resonances overlap but the methylene region of the ^{1}H NMR spectrum is quite clear and consists of four signals, two being associated with each isomer. Reducing the temperature to 223 K did not result in any significant difference in the ratio but some of the aromatic resonances separated, making identification of individual protons easier. All of the aromatic protons in the basal-apical isomers should be magnetically inequivalent because of the inequivalence of the two coordinating nitrogen atoms. As described above, we could not resolve individual resonances for all aromatic protons, but this may be due to the chemical shift differences being small. We attribute the smaller signals to a basal-apical isomer, which in the case of **2-edt** is computed to lie 6.9 kcal mol^{-1} higher in energy (Fig. S1).

Table 1. Selected structural parameters for 2,2′-bipy and 1,10-phen complexes (bond lengths in [Å] and bond angles in [°])

Compound	**1-edt**	**1-pdt**[11]	**2-edt**	**2-pdt**[10]	**2-adt**[9]
Fe–Fe	2.5318(5)	2.5623(4)	2.5321(6) 2.5298(6) 2.5227(6) 2.5221(6)	2.5483(4)	2.5354(8)
Fe–N	1.967(1)	1.982(2) 1.990(2)	1.971(2) 1.987(2) 1.969(2) 1.972(2) 1.962(2) 1.976(2) 1.962(2) 1.977(2)	1.986(2) 1.993(2)	1.989(3) 1.983(3)
Fe–Fe–N	100.69(4)	107.95(4) 105.34(4)	99.67(2) 102.54(7) 99.99(7) 102.44(7) 99.93(7) 101.74(7) 99.06(7) 102.05(7)	105.33(4) 104.89(5)	102.76(9) 101.55(9)
N–Fe–N	81.41(8)	80.81(6)	81.7(1) 82.3(1) 82.4(1) 82.2(1)	81.71(7)	81.8(2)

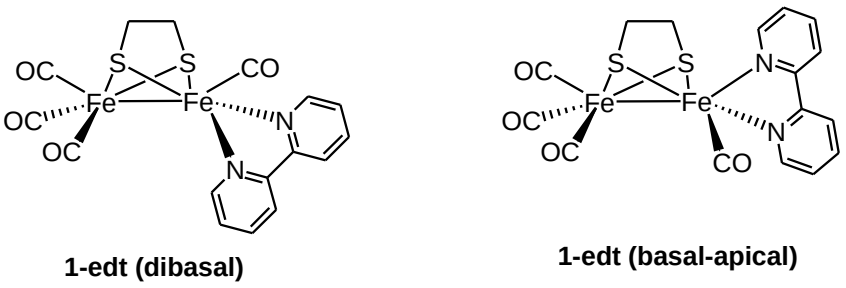

1-edt (dibasal) **1-edt (basal-apical)**

Chart 2. Dibasal and apical-basal isomers of $[Fe_2(CO)_4(\kappa^2\text{-}2,2'\text{-bipy})(\mu\text{-edt})]$ (**1-edt**).

Evidence of isomers is also seen in the IR spectrum of **1-edt**, which is more complex than that of **2-edt**. Specifically, two overlapping high-energy absorptions are seen at 2023 and 2010 cm^{-1}, the latter being somewhat larger. Comparison of these values with that of 2010 cm^{-1} for **2-edt** permits us to conclude that the absorption band at 2010 cm^{-1} in **1-edt** is associated with the dibasal isomer. In contrast, both IR and NMR data suggest only the presence of the dibasal isomer in solution for **1-pdt**.[11] Unlike **1-edt**, the solution IR

spectrum of **1-pdt** shows only three bands at 2007, 1937 and 1896 cm^{-1}, characteristic of the dibasal isomer.[11] Given that IR frequencies are (to some extent) a measure of electron-density on the diiron centre, this suggests that the 2,2′-bipy ligand in the dibasal position acts as a better σ-donor, creating a relatively electron-rich centre as compared to the basal-apical isomer. While related isomerism has been observed in diphosphine complexes of this type,[57-59] this does not lead to significantly different NMR spectra. The difference observed here may be important to later studies relating to the protonation and oxidation-reduction of the complex (*vide infra*). For example, protonation and oxidation are likely to be more favourable for the relatively electron-rich dibasal isomer, while reduction may be favoured for the apical-basal isomer.

Protonation studies

Schollhammer and co-workers [8] have shown that addition of $HBF_4{\cdot}Et_2O$ to a CH_2Cl_2 solution of **2-pdt** at low temperatures results in the formation of a bridging hydride complex, $[Fe_2(CO)_4(\mu\text{-}H)(\kappa^2\text{-}1,10\text{-phen})(\mu\text{-pdt})][BF_4]$ (**$2H^+$-pdt**). This has been crystallographically characterized but shows poor stability in solution at room temperature. Similarly, Jones and co-workers [11] have reported that **1-pdt** protonates slowly (*ca.* 6 mins) upon addition of $HBF_4{\cdot}Et_2O$ in MeCN to afford $[Fe_2(CO)_4(\mu\text{-}H)(\kappa^2\text{-}2,2'\text{-bipy})(\mu\text{-pdt})][BF_4]$ (**$1H^+$-pdt**). Addition of $HBF_4.Et_2O$ to CH_2Cl_2 solutions of **1-edt** and **2-edt** lead to rapid consumption of the neutral complexes consistent with protonation, new IR bands at 2102, 2050 and 1990 cm^{-1} for **1-edt**, while addition to **2-edt** gave the rapid appearance of three new absorptions at 2102, 2047 and 1989 cm^{-1}, which over a few minutes were replaced by absorptions at 2108, 2063, 2048 and 2018 cm^{-1}. Unfortunately, extensive and rapid decomposition of the generated products lead us to abandon this acid. Addition of two equivalents of CF_3CO_2H to **1-edt** in CH_2Cl_2 at room temperature led to an immediate change in colour from green to red with the complete disappearance of **1-edt** and the appearance of new absorptions at 2098, 2093, 2077, 2039, 2027, 1992 and 1973 cm^{-1} (Fig. S2a). Over a few minutes, the (small) absorption at 2077 cm^{-1} disappeared, while the other six bands remained, diminishing slowly over *ca.* 90 minutes. Similar observations were noted for **2-edt** (Fig. S2b). Thus, we believe that the diiron centre in both **1-edt** and **2-edt** is rapidly protonated by strong acids. The new absorption bands compare well with those of 2098, 2043 and 1985 cm^{-1} associated with **$2H^+$-pdt**[10] and 2098, 2044 and 1970 cm^{-1} for **$1H^+$-pdt**[11]. We attempted to follow the protonation of **1-edt** and **2-**

edt by ^{1}H NMR spectroscopy but in both cases after addition of acid all signals broadened significantly and no hydride signal could be observed[1]. We realise that this could be the result of protonation at sulfur, which has been proposed to occur upon addition of $HBF_4{\cdot}Et_2O$ to $[Fe_2(CO)_4(\kappa^2\text{-dppp})(\mu\text{-}SC_6H_2Cl_2S)]$ in CH_2Cl_2[60] and addition of HOTf to $[Fe_2(CO)_4(PMe_3)_2\{SCH_2N(C_6H_4\text{-}p\text{-}NO_2)CH_2S\}]$ in MeCN[61], although in neither case has the SH proton being observed by NMR or has crystallographic confirmation been obtained. Further, an average IR shift of +63 cm^{-1} is found for sulfur protonation of $[Fe_2(CO)_4(\kappa^2\text{-dppp})(\mu\text{-}SC_6H_2Cl_2S)]$ but +130 cm^{-1} for $[Fe_2(CO)_4(PMe_3)_2\{SCH_2N(C_6H_4\text{-}p\text{-}NO_2)CH_2S\}]$, making protonation at sulfur impossible to determine on the basis of IR data. We thus favour, based on the similarity of our IR observations with those of Schollhammer[10] and Jones[11] and the crystallographic characterisation of $[Fe_2(CO)_4(\mu\text{-H})(\kappa^2\text{-1,10-phen})(\mu\text{-pdt})][BF_4]$ (**2H$^+$-pdt**)[10], formation of $[Fe_2(CO)_4(\mu\text{-H})(\kappa^2\text{-2,2′-bipy})(\mu\text{-edt})]^+$ (**1H$^+$-edt**) and $[Fe_2(CO)_4(\mu\text{-H})(\kappa^2\text{-1,10-phen})(\mu\text{-edt})]^+$ (**2H$^+$-edt**) upon addition of CF_3CO_2H. Dibasal and basal-apical isomers are possible (Scheme 2) and DFT calculations on **2H$^+$-edt** confirm that the dibasal isomer is 3.0 kcal mol^{-1} more stable than its apical-basal counterpart.

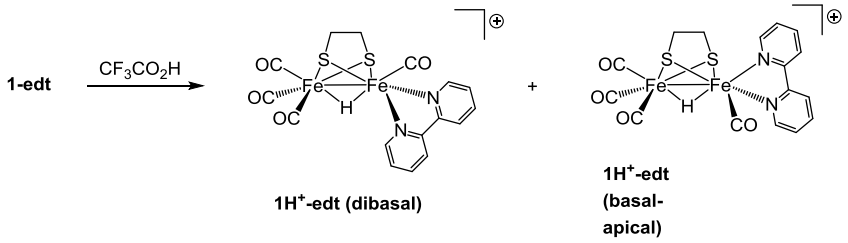

Scheme 2. Possible isomers of $[Fe_2(CO)_4(\kappa^2\text{-2,2′-bipy})(\mu\text{-edt})]$ (**1H$^+$-edt**).

Electrochemistry

The redox behaviour of **1-edt** and **2-edt** were studied in MeCN by cyclic voltammetry. Both show an irreversible reduction wave at E_p = –2.05 V, together with an irreversible oxidative wave at E_p = –0.18 V, suggesting that the nature of the diamine has little electronic impact upon the diiron core (Fig. 2). Peak currents for **1-edt** are consistently larger than those for **2-edt**, which is also observed for the free diamines that show a single reduction wave at E_p = –

[1] We have also observed similar behaviour for $[Fe_2(CO)_4(\kappa^2\text{-dppe})(\mu\text{-edt})]$, addition of acid leads to IR changes consistent with formation of $[Fe_2(CO)_4(\mu\text{-H})(\kappa^2\text{-dppe})(\mu\text{-edt})]^+$ (akin to those noted for the corresponding pdt complex[58]) but we were unable to identify a hydride resonance by ^{1}H NMR spectroscopy.

2.63 V (2,2′-bipy) and E_p = –2.46 V (1,10-phen), respectively (Fig. S3). Jones and co-workers investigated the electrochemistry of $[Fe_2(CO)_4(\kappa^2\text{-}2,2'\text{-bipy})(\mu\text{-pdt})]$ (**1-pdt**) under similar conditions and showed by controlled-potential coulometry that the irreversible reduction at E_p = –2.06 V is a two-electron process, and suggested that one electron is associated with the diiron centre and the second with the 2,2′-bipy ligand.[11] This is consistent with the reduction potentials of the free diamines that are expected to show a positive shift due to the removal of electron density upon coordination to iron (Fig. S3). A plot of the current function ($i_p/\sqrt{\nu}$), associated with the reduction of **1-edt** and **2-edt**, against scan rate (ν) shows that it deviates from linearity only at very slow scan rates, i.e. the electrode process tends towards a one-electron transfer on the shorter time scale, otherwise the reductions are two-electron electrode processes (Fig. S4). No significant change has been observed on the CVs of the two complexes when the scan rate is varied (0.025 to 1 V/s) (Figs. S5 and S6).

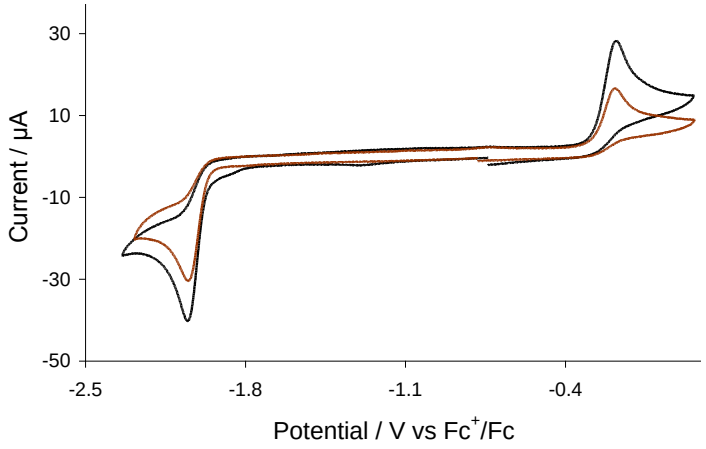

Fig. 2. CVs of $[Fe_2(CO)_4(\kappa^2\text{-}2,2'\text{-bipy})(\mu\text{-edt})]$ (**1-edt**) (black) and $[Fe_2(CO)_4(\kappa^2\text{-}1,10\text{-phen})(\mu\text{-edt})]$ (**2-edt**) (brown) in MeCN (1 mM solution, supporting electrolyte $[NBu_4][PF_6]$, scan rate 0.1 Vs^{-1}, glassy carbon electrode, potential vs Fc^+/Fc).

The diiron centre in both **1-edt** and **2-edt** is oxidized irreversibly at E_p = –0.18 V. The nature of this has been probed chemically using $[Cp_2Fe][BF_4]$ as the oxidant. Addition of one equivalent to a CH_2Cl_2 solution of **1-edt** or **2-edt** gave an instant colour change, from dark green to orange for **1-edt** and from dark blue to yellow for **2-edt**, concomitant with the appearance of new IR bands at 2106, 2100, 2060, 2048, 2023 cm^{-1} and 2106, 2100, 2062, 2048, 2026 cm^{-1} associated with the formation of **1-edt**$^+$ and **2-edt**$^+$, respectively (Fig. S7). The intensity of these bands relative to those of the starting materials is relatively low, and all absorptions disappeared over a few minutes. This is consistent with the irreversible nature of

the electrochemical oxidation. On the basis of the IR data, we cannot fully assign the structures of these oxidized species but as the lowest energy absorptions are at 2023-2026 cm^{-1}, it would appear that a semi-bridging carbonyl ligand has not been generated.

Density functional theory (DFT) calculations

In order to understand the sequence and consequences of electron addition to these complexes we have carried out a series of DFT calculations on **2-edt**, (**2-edt**)$^{-}$ and (**2-edt**)$^{2-}$. Initially we optimized the ground-state structure of **2-edt**, and the obtained structural parameters agree well with those of the X-ray crystal structure (Fig. S8). The major component of the HOMO is the iron-iron bonding orbital (Fig. 3, left) which is consistent with the 96 cm^{-1} blue shift of the highest energy CO-absorption after chemical oxidation with $[Cp_2Fe][BF_4]$. The LUMO of **2-edt** is predominantly 1,10-phen π^* character in nature but also has a small iron-iron anti-bonding component (Fig. 3, right). The calculated iron-iron bond length of 2.558 Å is close to that of 2.548(1) Å (av.) found in the solid state.

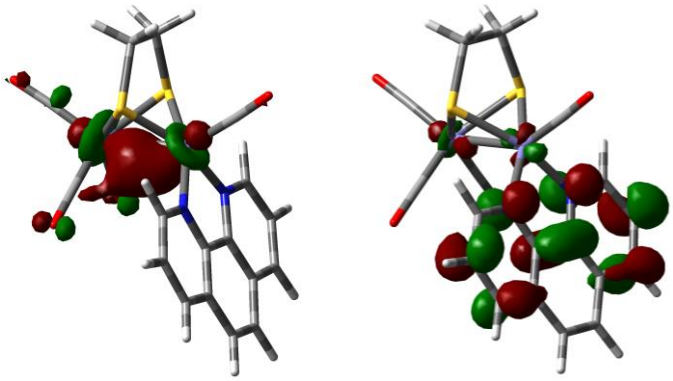

Fig. 3. HOMO (left) and LUMO (right) of $[Fe_2(CO)_4(\kappa^2\text{-}1,10\text{-phen})(\mu\text{-edt})]$ (**2-edt**). The contour plots are printed at an isovalue of 0.55.

The addition of an electron to the LUMO affords the radical anion **2-edt**$^{-}$, and the orbital composition of the SOMO looks very much like the LUMO of **2-edt** (Fig. S9). The small degree of antibonding character in the Fe–Fe bond of **2-edt**$^{-}$ results in a slight elongation of the Fe-Fe bond by ~0.12 Å to 2.678 Å relative the neutral parent. The Wiberg bond indices for the Fe–Fe bonds in **2-edt** and **2-edt**$^{-}$ are 0.42 and 0.32, respectively, and the 24% reduction in the bond order indicates that while the SOMO is primarily phenanthroline-based there is also some diiron character. The addition of the second electron affords **2-edt**$^{2-}$ whose

most stable configuration corresponds to the open-shell triplet; the closed-shell singlet state is less stable by 4.2 kcal mol^{-1} and attempts to optimize the structure for an open-shell triplet were not successful, collapsing to the aforementioned singlet. The SOMO (Fig. 4, right) is very similar in nature to the SOMO of **2-edt**$^{-}$, being mainly phenanthroline-based. The second singly occupied orbital, SOMO-1 (Fig. 4, left), lies *ca.* 12 kcal mol^{-1} lower in energy and is predominantly iron-iron σ* in nature. Thus, the second electron populates a metal-based orbital, and this electron accession results in a lowering of the energy of the antibonding Fe-Fe orbital relative to that of the ligand-based SOMO. A result of the population of the primarily metal-based orbital is the severe elongation of the Fe–Fe vector, being calculated at 3.214 Å in **2-edt**$^{2-}$, and whose Wiberg bond index of 0.087 signals minimal bonding interaction between the iron atoms. Thus upon addition of the second electron there is a significant structural change, leading to cleavage of the iron-iron bond.

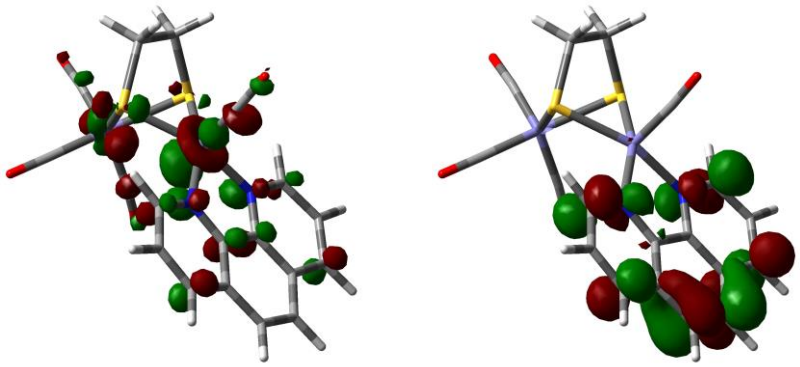

Fig. 4. SOMO-1 (left) and SOMO (right) of $[Fe_2(CO)_4(\kappa^2\text{-}1,10\text{-phen})(\mu\text{-edt})]^-$ (**2-edt**$^{2-}$). The contour plots are printed at an isovalue of 0.55.

Electrocatalytic studies

Electrocatalytic proton reduction effected by **1-edt** (Fig. 5) and **2-edt** (Fig. 6) was investigated in MeCN using CF_3CO_2H as the proton source. Attempts to study the catalysis using stronger acids, *e.g.* $HBF_4{\cdot}Et_2O$ or *p*-toluenesulfonic acid (*p*-TsOH), which were used for the catalytic study of **1-pdt**, were unsuccessful as both **1-edt** and **2-edt** degrade rapidly in the presence of these acids. Upon addition of one molar equivalent of CF_3CO_2H, CVs of both complexes show two new reduction peaks (at –1.68 and –1.89 V for **1-edt** and at –1.70 and –1.98 V for **2-edt**) in addition to the peak at –2.05 V. All three peaks grow with increasing

acid concentration, which is characteristic of electrocatalytic proton reduction. However, the catalytic peak seen at the reduction potential of the neutral complexes (–2.05 V) disappears as the concentration of acid is increased (> 6 equivalents for **1-edt** and > 2 equivalents for **2-edt**). This is in contrast with the results obtained for **1-pdt**, for which the catalytic peak at the reduction potential of the neutral species was the prominent reduction feature throughout the experiment. This can be explained by comparing the rate of protonation of the edt and pdt complexes. While **1-pdt** undergoes slow protonation in the presence of strong acid ($HBF_4{\cdot}Et_2O$; pK_a ≈ 0.1 in MeCN)[62], protonation of the edt complexes are relatively fast even in the presence of CF_3CO_2H (pK_a ≈ 12.7 in MeCN)[62].

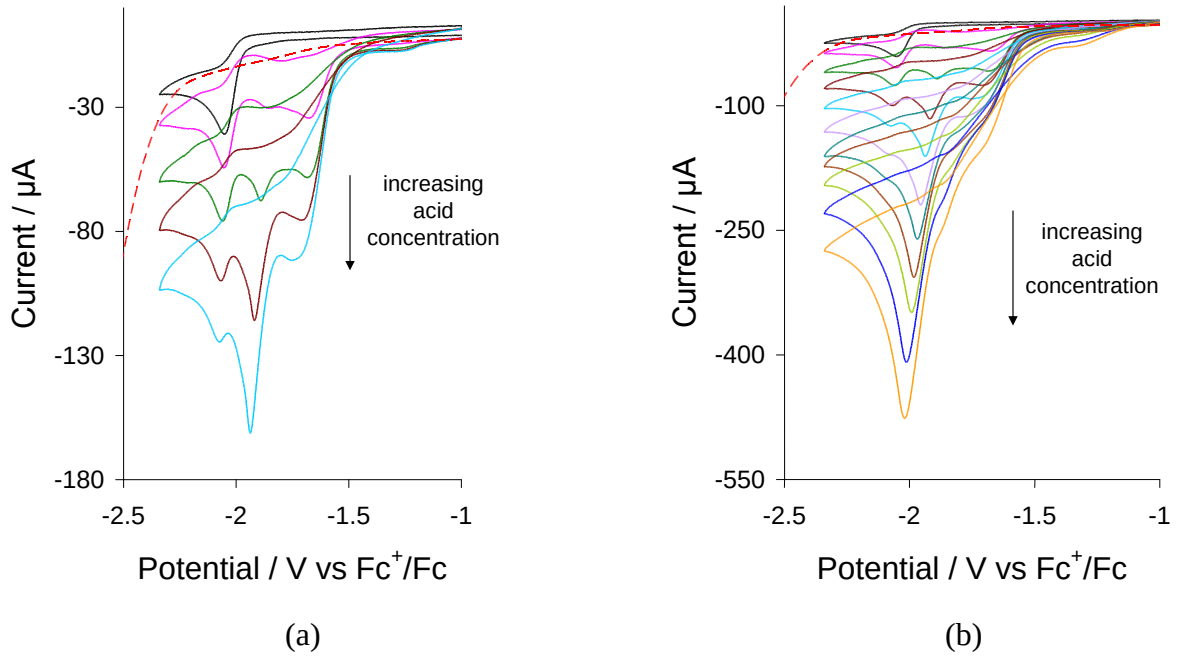

Fig. 5. CVs of $[Fe_2(CO)_4(\kappa^2\text{-}2,2'\text{-bipy})(\mu\text{-edt})]$ (**1-edt**) - (a) upon addition of 1-4 equivalents of CF_3CO_2H, (b) upon addition of 1-10 equivalents of CF_3CO_2H (in MeCN, 1 mM solution, supporting electrolyte $[NBu_4][PF_6]$, scan rate 0.1 Vs^{-1}, glassy carbon electrode, potential vs Fc^+/Fc). Response of 10 equivalents CF_3CO_2H alone is shown with the red dashed line.

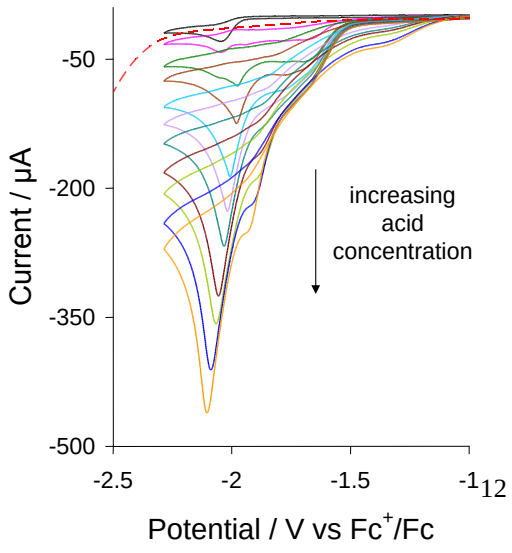

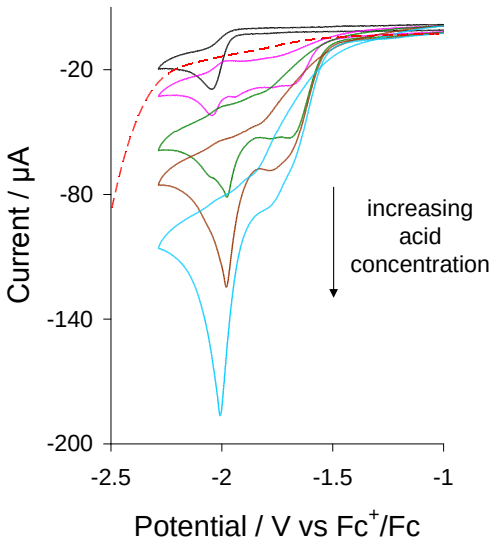

(a) (b)

Fig. 6. CVs of $[Fe_2(CO)_4(\kappa^2\text{-}1,10\text{-phen})(\mu\text{-edt})]$ (**2-edt**) - (a) upon addition of 1-4 equivalents of CF_3CO_2H, (b) upon addition of 1-10 equivalents of CF_3CO_2H (in MeCN, 1 mM solution, supporting electrolyte $[NBu_4][PF_6]$, scan rate 0.1 Vs^{-1}, glassy carbon electrode, potential vs Fc^+/Fc). Response of 10 equivalents CF_3CO_2H alone is shown with the red dashed line.

The first reduction peak in the CVs of **1-edt** and **2-edt** in the presence of one equivalent of CF_3CO_2H appears *ca.* 0.35V more positive than the reduction potential of the neutral species and are due to the reduction of protonated species (**1H$^+$-edt** and **2H$^+$-edt**) which are responsible for the catalytic current at this potential. The current of the first reduction peak levels off at higher acid concentration and reaches a plateau after addition of 6 equivalents of acid, which indicates an acid-independent rate-limiting step such as the liberation of H_2 under these conditions. In contrast, the second reduction wave increases linearly with acid concentration indicating another proton reduction process at this potential (Fig. S10).

The catalytic mechanism of **1-pdt** proposed by Jones and co-workers is shown in Scheme 3.[11] Since **1-pdt** is protonated slowly by a strong acid ($HBF_4{\cdot}Et_2O$), these authors suggest that both **1H$^+$-pdt** and **1H-pdt** are the active electrocatalytic species in solution. Although IR spectroscopic data suggest rapid protonation of **1-edt** and **2-edt** by CF_3CO_2H, the CVs show that some **1-edt** is present in solution at low acid concentrations, and it undergoes complete protonation only after addition of 7 equivalents of acid in the electrochemical cell. This can be attributed to the presence of a large amount of electrolyte, $[Bu^t_4N][PF_6]$, in the electrochemical cell that reduces the strength of the acid. Thus we propose that **1-edt** follows the same mechanism proposed for **1-pdt** (Scheme 3) at low acid concentrations, but it follows

a different mechanism at high acid concentration when **1-edt** undergoes rapid protonation by CF_3CO_2H (see below Scheme 4).

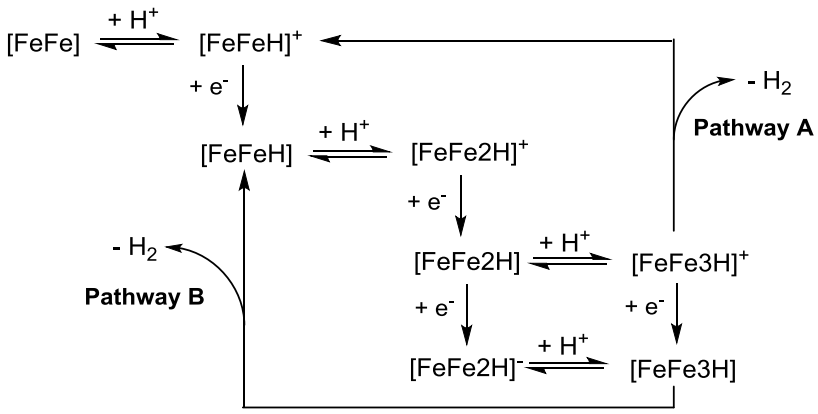

Scheme 3. Proposed mechanisms for the electrocatalytic proton reduction by $[Fe_2(CO)_4(\kappa^2\text{-}2,2'\text{-bipy})(\mu\text{-pdt})]$ (**1-pdt**).[11]

In contrast, the peak at the reduction potential of **2-edt** disappears after addition of 3 equivalents of CF_3CO_2H and the CV shows two reduction peaks associated with **$2H^+$-edt**. Since **2-edt** undergoes relatively rapid protonation at low concentration of CF_3CO_2H, even in the presence of a large amount of electrolyte that reduces the strength of CF_3CO_2H, we surmise that it follows a different, but relatively simple, mechanism for electrocatalytic proton reduction that is shown in Scheme 4. According to this mechanism, H_2 evolution at the first reduction potential takes place *via* either CECE or CEEC pathways (Scheme 4). The neutral complex undergoes protonation, followed by reduction, to form the neutral hydride species **[FeFeH]**. This can then either react with a second proton followed by reduction at a low potential, or undergo a further reduction at a more negative potential before reacting with a second proton, which accounts for the reduction of protons at the potential of the second catalytic wave (Scheme 4). However, at low acid concentrations, due to the slow rate of protonation, some **1-edt** is present and it will follow the same EECC mechanism that has been proposed for **1-pdt**[11] (Scheme 5). Electrocatalysis of **1-edt** and **2-edt** with $HBF_4{\cdot}Et_2O$ were unsuccessful since both degrade upon addition of a slight excess of $HBF_4{\cdot}Et_2O$ into the electrochemical cell.

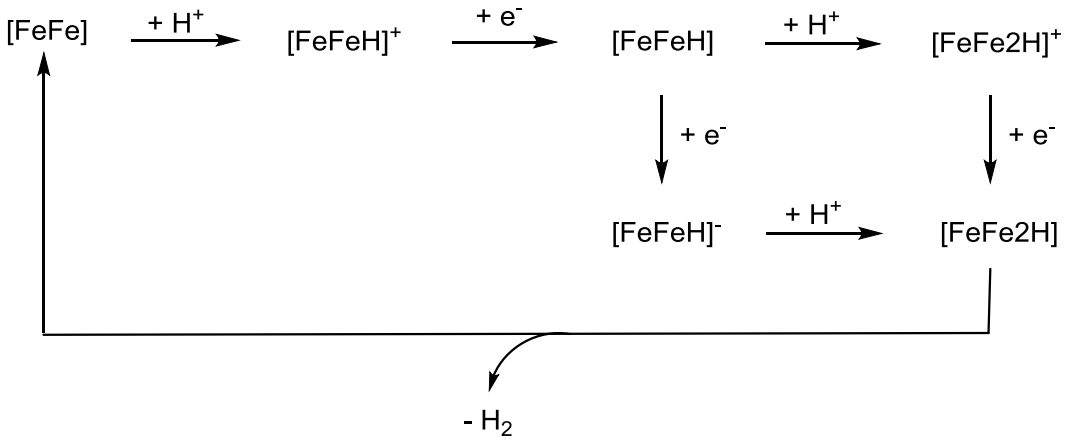

Scheme 4. Proposed mechanism for the electrocatalytic proton reduction by $[Fe_2(CO)_4(\kappa^2\text{-}2,2'\text{-bipy})(\mu\text{-edt})]$ (**1-edt**) and $[Fe_2(CO)_4(\kappa^2\text{-}1,10\text{-phen})(\mu\text{-edt})]$ (**2-edt**).

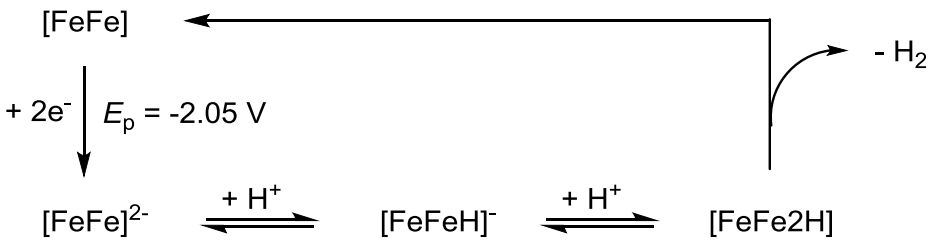

Scheme 5. Proposed mechanism for the catalytic event at the reduction potential of $[Fe_2(CO)_4(\kappa^2\text{-}2,2'\text{-bipy})(\mu\text{-edt})]$ (**1-edt**) during electrocatalytic proton reduction at low acid concentrations.[11]

Since the cationic hydrides **1H$^+$-edt** and **2H$^+$-edt** are the dominant active electrocatalytic species in solution for these edt complexes, we have calculated the ground state electronic structures of **2H$^+$-edt** in order to get insight into the role of the diamine in the catalysis, since the ligand is involved in the two-electron reduction process of the neutral complexes. As discussed above, both **1H$^+$-edt** and **2H$^+$-edt** can exist in two isomeric forms (apical-basal and dibasal) when protonation is carried out by CF_3CO_2H. The ground state electronic structure of both isomers of **2H$^+$-edt** have been calculated by DFT methods (Figs. S11 and S12). Although the energies of the frontier orbitals of the isomers are quite similar, the orbital composition is different. The HOMO of the dibasal isomer contains π character from the 1,10-phen ligand whereas that of the apical-basal isomer is primarily a metal-based orbital with the largest iron contribution originating at the 1,10-phen-substituted iron center. Interestingly, the opposite situation is observed for the LUMOs of these isomers, which indicates that the frontier orbitals of these cationic hydrides undergo orbital inversion when

the diamine moves from dibasal to apical-basal conformation, and vice-versa. Calculations also show that the energy required for the conversion of the apical-basal isomer to the dibasal isomer is > 35 kcal mol^{-1}, which is very high, and a simple tripodal rotation of the ligands at the Fe(CO)(phen) moiety is not energetically feasible by this path. Thus, we assume that electron transfer to the diiron core during catalysis, involving the cationic hydrides **1H$^+$-edt** and **2H$^+$-edt** as the active species in solution, also occurs (at least partially) via the diamine ligands, a phenomenon that is also observed when the neutral complexes **1-edt** and **2-edt** are the only active catalytic species in solution (Scheme 5).

Conclusions

The diiron complexes $[Fe_2(CO)_4(\kappa^2\text{-}2,2'\text{-bipy})(\mu\text{-edt})]$ (**1-edt**) and $[Fe_2(CO)_4(\kappa^2\text{-}1,10\text{-phen})(\mu\text{-edt})]$ (**2-edt**) have been synthesized in moderate yields, and their crystal structures show that the diamine occupies basal sites in the solid-state for both complexes, while both dibasal and apical-basal isomers are present in solution. This is in contrast with what is observed for their pdt analogues, which exist only in dibasal form both in the solid state and in solution.[10,11] We suggest that in **1-pdt** and **2-pdt**, the non-bonding interactions between the diamine ligand and the extra methylene group of the dithiolate backbone prevents the formation of the apical-basal isomer. Both **1-edt** and **2-edt** readily protonate, but the protonated products show limited stability in the presence of air. Protonated **1H$^+$-edt** and **2H$^+$-edt** probably exist in both dibasal and apical-basal forms in the presence of moderately strong acid (CF_3CO_2H), while a single isomer is observed when strong acid ($HBF_4{\cdot}Et_2O$) is used as the proton source, indicating that the rate of conversion to the thermodynamically more stable isomer depends on the strength of acid.

Both **1-edt** and **2-edt** show single irreversible oxidation and reduction waves at E_p = –0.18 V and E_p = –2.05 V, respectively, in MeCN, the latter being proposed to be a two-electron process with one electron being associated with the diiron centre and the second with the diamine ligand, a feature also proposed for **1-pdt**.[11] DFT calculations on **2-edt** show that the first electron goes onto the phenanthroline ligand in an orbital with significant π* character. The addition of the second electron affords an open-shell triplet dianion upon the population of an orbital with significant Fe-Fe σ* character. This leads to significant lengthening of the iron-iron bond and possibly accounts for the observed irreversible two-electron reduction of

2-edt resulting from structure-induced orbital inversion. The proton reduction ability of the complexes has been studied in MeCN using CF_3CO_2H as the proton source. These show that both complexes are able to catalyse proton reduction in the presence of the moderately strong acid CF_3CO_2H, but the catalytic pathways differ due to the relative ease of protonation. This leads to different mechanisms for proton reduction by 2,2′-bipy and 1,10-phen complexes, owing to the different rates of protonation. At low acid concentrations, due to the slow protonation of **1-edt**, both **1H$^+$-edt** and **1H-edt** are proposed to be the active electrocatalytic species, a scenario that is similar to that proposed for **1-pdt**. In contrast, rapid protonation of **2-edt** even at low acid concentrations suggests that **2H$^+$-edt** is the only active catalytic species during electrocatalytic proton reduction. Theoretical studies indicate that electron transfer to the diiron core during catalysis always occurs (at least partially) via the diamine ligands in all scenarios. This study reveals that although the electronic impact of both 2,2′-bipy and 1,10-phen on the diiron core are similar, the resultant diiron complexes undergo protonation at different rates, which significantly influence the catalytic pathways followed. This may to some extent be a result of the interaction between redox-active diiron and ligand centres although further work is required to fully establish this.

Experimental section

General

Unless otherwise noted, all the reactions were carried out under a nitrogen atmosphere using standard Schlenk techniques. Reagent-grade solvents were dried using appropriate drying agents and distilled prior to use by standard methods. Infrared spectra were recorded on a Shimadzu FTIR 8101 or Nicolet 6700 FT-IR spectrophotometer. NMR spectra were recorded on a Bruker DPX 400 instrument. Elemental analyses were performed by Microanalytical Laboratories, University College London and $[Fe_2(CO)_6(\mu\text{-edt})]$ was prepared by literature methods.[63]

Synthesis of $[Fe_2(CO)_4(\kappa^2\text{-}2,2'\text{-bipy})(\mu\text{-edt})]$ (1-edt)

To an MeCN solution (15 mL) of $[Fe_2(CO)_6(\mu\text{-edt})]$ (100 mg, 0.269 mmol) was added 2,2′-bipy (42 mg, 0.269 mmol) and $Me_3NO{\cdot}2H_2O$ (37 mg, 0.333 mmol) and the mixture was

heated at boiling temperature for 1 h. The reaction mixture was cooled to room temperature, and its volume was reduced to 3-4 mL by rotary evaporation. The mixture was passed through a short silica column (6 cm) using CH_2Cl_2 as eluent to remove unreacted Me_3NO and other undissolved materials. The solution was then transferred into a 100 mL round-bottomed flask and again concentrated to 3-4 mL. The addition of a layer of cold hexane over this solution and cooling at –20 °C for several days gave dark green crystals of $[Fe_2(CO)_4(\kappa^2\text{-}2,2'\text{-bipy})(\mu\text{-edt})]$ (**1-edt**) (56 mg, 44%). IR ($\nu_{(CO)}$, CH_2Cl_2): 2023m, 2010vs, 1938vs, 1900m, 1859w cm^{-1}; ^1H NMR ($CDCl_3$): δ 8.87 (d, J 4.4, 2H, major), 8.31 (d, J 2.7, 2H, minor), 8.29 (d, J 8.4, 2H, minor), 8.11 (d, J 7.5, 2H, major), 7.93 (t, J 4.1, 2H, minor), 7.79 (t, J 4.5, 2H, major), 7.26 (brs, 2H, major + minor), 2.40 (apparent d, J 7.6, 2H, minor), 2.28 (apparent d, J 7.6, 2H, minor), 2.20 (apparent d, J 7.0, 2H, major), 2.05 (apparent d, J 7.0, 2H, major); Anal. calc. for $Fe_2N_2S_2O_4C_{16}H_{12}.0.5CH_2Cl_2$: C, 38.47, N, 5.44, H, 2.52; Found C, 38.93, N, 5.51, H, 2.42.

Synthesis of $[Fe_2(CO)_4(\kappa^2\text{-}1,10\text{-phen})(\mu\text{-edt})]$ (2-edt)

An MeCN solution (15 mL) of $[Fe_2(CO)_6(\mu\text{-edt})]$ (100 mg, 0.269 mmol), 1,10-phen (49 mg, 0.272 mmol) and $Me_3NO{\cdot}2H_2O$ (37 mg, 0.333 mmol) was heated at boiling temperature for 1.5 h. A similar workup described as above gave dark green crystals of $[Fe_2(CO)_4(\kappa^2\text{-}1,10\text{-phen})(\mu\text{-edt})]$ (**2-edt**) (43 mg, 32%). IR ($\nu_{(CO)}$, CH_2Cl_2): 2010vs, 1938s, 1900m cm^{-1}; ^1H NMR ($CDCl_3$): δ 9.14 (d, J 5.3, 2H, major), 8.63 (d, J 5.3, minor), 8.43 (d, J 7.8, minor), 8.30 (d, J 7.9, 2H, major), 8.06 (s, minor), 7.96 (s, 2H, major), 7.65 (dd, J 7.9, 5.3, 2H, major), 2.46 (m, minor), 2.26 (apparent dt, J 7.3, 5.0, 2H, major), 2.11 (apparent dt, J 7.4, 3.8, 2H, major); Anal. calc. for $Fe_2N_2S_2O_4C_{18}H_8.2CH_2Cl_2$: C, 36.03, N, 4.20, H, 2.40; Found C, 35.65, N, 4.69, H, 2.19.

Protonation of 1-edt and 2-edt

2 molar equivalents of CF_3CO_2H (0.8 μL) was added to a dichloromethane solution of **1-edt** (2.4 mg, 0.005 mmol) or **2-edt** (2.5 mg, 0.005 mmol) at room temperature. The resulted solution was then transferred into a solution IR cell fitted with calcium fluoride plates, and a series of spectra were recorded as a function of time.

Chemical oxidation of 1-edt and 2-edt with $[Cp_2Fe][BF_4]$

1 molar equivalents of $[Cp_2Fe][BF_4]$ (1.4 mg, 0.005 mmol) was added to a dichloromethane solution of **1-edt** (2.4 mg, 0.005 mmol) or **2-edt** (2.5 mg, 0.005 mmol) at room temperature. The resulted solution was then transferred into a solution IR cell fitted with calcium fluoride plates, and a series of spectra were recorded as a function of time.

Electrochemical Studies

Electrochemistry was carried out either in deoxygenated MeCN with 0.1 M $TBAPF_6$ as the supporting electrolyte. All CVs were obtained using a conventional three-electrode cell setup under an argon atmosphere. The working electrode was a 3 mm diameter glassy carbon electrode that was polished with 0.3 μm alumina slurry prior to each scan. The counter electrode was a Pt wire, and the quasi-reference electrode was a silver wire. All CVs were referenced to the Fc^+/Fc redox couple. An Autolab potentiostat (EcoChemie, Netherlands) was used for all electrochemical measurements. Catalysis studies were carried out by adding equivalents of CF_3CO_2H (Sigma-Aldrich).

Crystal structure determination of 1-edt and 2-edt

Single crystals of **1-edt** and **2-edt** were mounted on glass fibres, and all geometric and intensity data were taken from these samples using a Bruker SMART APEX CCD diffractometer using graphite-monochromated Mo-Kα radiation (λ = 0.71073 Å) at 150 ± 2 K. Data collection, indexing and initial cell refinements were all done using SMART software.[64] Data reduction were carried out with SAINT PLUS,[65] and absorption corrections applied using the programme SADABS[66]. Structures were solved by direct methods and developed using alternating cycles of least-squares refinement and difference-Fourier synthesis. All non-hydrogen atoms were refined anisotropically. Hydrogen atoms were located from difference maps and refined isotropically. Structure solution used SHELXTL PLUS V6.10 program package.[67]

Crystallographic data for **1-edt**: dark green block, dimensions 0.34 × 0.14 × 0.11 mm^3, orthorhombic, space group *Pnma*, a = 13.015(1), b = 12.264(1), c = 10.759(1) Å, α = 90, β = 90, γ = 90°, V = 1717.4(3) $Å^3$, Z = 4, F(000) 952, d_{calc} = 1.826 g cm^{-3}, μ = 1.958 mm^{-1}. 13580

reflections were collected, 2191 unique [R(int) = 0.0308]. At convergence, R_1 = 0.0249, wR_2 = 0.0609 [$I > 2.0\sigma(I)$] and R_1 = 0.0268, wR_2 = 0.0618 (all data), for 151 parameters.

Crystallographic data for **2-edt**: dark green block, dimensions 0.32 × 0.18 × 0.16 mm^3, triclinic, space group $P\bar{1}$, a = 10.6863(9), b = 18.224(2), c = 20.886(2) Å, α = 112.523(1), β = 101.945(1), γ = 92.294(1)°, V = 3643.6(5) $Å^3$, Z = 8, F(000) 2000, d_{calc} = 1.809 g cm^{-3}, μ = 1.850 mm^{-1}. 31408 reflections were collected, 16665 unique [R(int) = 0.0264]. At convergence, R_1 = 0.0426, wR_2 = 0.1242 [$I > 2.0\sigma(I)$] and R_1 = 0.0583, wR_2 = 0.1410 (all data), for 1009 parameters.

Density functional theory (DFT) calculations

All calculations were performed with the hybrid DFT functional B3LYP, as implemented by the Gaussian 09 program package.[68] This functional utilizes the Becke three-parameter exchange functional (B3),[69] combined with the correlation functional of Lee, Yang and Parr (LYP).[70] The iron atoms were described by Stuttgart–Dresden effective core potentials (ecp) and a SDD basis set, while the 6-31+G(d′) basis set, as implemented in the Gaussian09 program suite, was employed for the remaining atoms. The geometry-optimized structures contain zero imaginary. The computed frequencies were used to make zero-point and thermal corrections to the electronic energies; the reported free energies are quoted in kcal mol^{-1}. The natural charges and Wiberg bond indices reported here were computed using Weinhold's natural bond orbital (NBO) program, as executed by Gaussian 09.[71,72] The geometry-optimized structures have been drawn with the JIMP2 molecular visualization and manipulation program.[73,74]

Acknowledgements

We thank the Commonwealth Scholarship Commission and the European Union (Erasmus Mundus) for scholarships to SG and AR respectively. GH and EN thank The Royal Society for an International Exchange Award in the area of proton reduction catalysis. MGR acknowledges financial support from the Robert A. Welch Foundation (Grant B-1093) and computational resources through UNT's High-Performance Computing Services and

CASCaM. Prof. Michael B. Hall (TAMU) is thanked for providing us a copy of his JIMP2 program, which was used to prepare the geometry optimized structures reported here.

Appendix A. Supplementary data

Additional electrochemical and computational information are given in Figs. S1-S12. CCDC 1454073 and 1454074 contain the supplementary crystallographic data for **1-edt** and **2-edt** respectively. These data can be obtained free of charge via http://www.ccdc.cam.ac.uk/conts/retrieving.html, or from the Cambridge Crystallographic Data Centre, 12 Union Road, Cambridge CB2 1EZ, UK; fax: (+44) 1223-336-033; or e-mail: deposit@ccdc.cam.ac.uk

References

(1) J.M. Camara, T.B. Rauchfuss, Nat. Chem., 2012, **4**, 26-30.

(2) C. Tard, X.M. Liu, S.K. Ibrahim, M. Bruschi, L. De Gioia, S.C. Davies, X. Yang, L.S. Wang, G. Sawers, C.J. Pickett, Nature, 2005, **433**, 610-613.

(3) C. Greco, Inorg. Chem., 2013, **52**, 1901-1908.

(4) Y. Si, K. Charreteur, J.-F. Capon, F. Gloaguen, F.Y. Pétillon, P. Schollhammer, J. Talarmin, J. Inorg. Biochem., 2010, **104**, 1038-1042.

(5) C. Gimbert-Suriñach, M. Bhadbhade, S. B. Colbran, Organometallics, 2012, **31**, 3480-3491.

(6) J.-F. Capon, F. Gloaguen, F. Y. Pétillon, P. Schollhammer, J. Talarmin, Eur. J. Inorg. Chem., 2008, 4671-4681.

(7) C. Greco, L. De Gioia, Inorg. Chem., 2011, **50**, 6987–6995.

(8) P.-Y. Orain, J.-F. Capon, F. Gloaguen, F.Y. Pétillon, P. Schollhammer, J. Talarmin, G. Zampella, L. De Gioia, T. Roisnel, Inorg. Chem., 2010, **49**, 5003-5008.

(9) S. Ezzaher, P.-Y. Orain, J.-F. Capon, F. Gloaguen, F. Pétillon, T. Roisnel, P. Schollhammer, J. Talarmin, Chem. Commun., 2008, 2547-2549.

(10) P.-Y. Orain, J.-F. Capon, N. Kervarec, F. Gloaguen, F. Pétillon, R. Pichon, P. Schollhammer, J. Talarmin, Dalton Trans., 2007, 3754-3756.

(11) S. Roy, T.L. Groy, A. K. Jones, Dalton Trans., 2013, **42**, 3843-3853.

(12) J. W. Peters, W. N. Lanzilotta, B. J. Lemon, L. C. Seefeldt, Science, 1998, **282**, 1853-1858.

(13) Y. Nicolet, C. Piras, P. Legrand, C. E. Hatchikian, J. C. Fontecilla-Camps, Structure 1999, **7**, 13-23.

(14) M. Bruschi, C. Greco, P. Fantucci, L. De Gioia, Inorg. Chem., 2008, **47**, 6056-6071.

(15) D. E. Schwab, C. Tard, E. Brecht, J. W. Peters, C. J. Pickett, R. K. Szilagyi, Chem. Commun., 2006, 3696-3698.

(16) (a) C. V. Popescu, E. Munck, J. Am. Chem. Soc., 1999, **121**, 7877-7884; (b) A. Adamska, A. Silakov, O. Rűdiger, E. Reijerse, W. Lubitz, C. Lambertz, T. Happe, Angew. Chem., Int. Ed., 2012, **51**, 11458-11462. (c) A. Adamska-Venkatesh, D. Krawietz, J. Siebel, K. Weber, T. Happe, E. Reijerse, W. Lubitz, *J. Am. Chem. Soc.*, 2014, **136**, 11339-11346.

(17) Y.-C. Liu, C.-H. Lee, G.-H. Lee, M.-H. Chiang, Eur. J. Inorg. Chem., 2011, 1155-1162.

(18) G. Chelucci, R. P. Thumme, Chem. Rev., 2002, **102**, 3129-3170.

(19) P. G. Sammes, G. Yahioglu, Chem. Soc. Rev., 1994, 327-334.

(20) C. V. Krishnan, C. Creutz, H. A. Schwarz, N. Sutin, J. Am. Chem. Soc., 1983, **105**, 5617-5623.

(21) M. H. Chisholm, J. C. Huffman, I. P. Rothwell, P. G. Bradley, N. Kress, W. H. Woodruff, J. Am. Chem. Soc., 1981, **103**, 4945-4947.

(22) E. Gore-Randall, M. Irwin, M. S. Denning, J. M. Goicoechea, Inorg. Chem., 2009, **48**, 8304-8316.

(23) L. Echegoyen, A. DeCian, J. Fischer, J.-M. Lehn, Angew. Chem., Int. Ed., 1991, **30**, 838-840.

(24) H. Bock, J.-M. Lehn, J.Pauls, S. Holl, V. Krenzel, Angew. Chem., Int. Ed., 1999, **38**, 952-955.

(25) P. L. Bellavance, E. R. Corey, J. Y. Corey, G. W. Hey, Inorg. Chem., 1977, **16**, 462-467.

(26) G. B. Nikiforov, H. W. Roesky, M. Noltemeyer, H.-G. Schmidt, Polyhedron, 2004, **23**, 561-566.

(27) M. Irwin, R. K. Jenkins, M. S. Denning, T. Krämer, F. Grandjean, G. J. Long, R. Herchel, J. E. McGrady, J. M. Goicoechea, Inorg. Chem., 2010, **49**, 6160-6171.

(28) D. Roitershtein, Ã. Domingos, L. C. J. Pereira, J. R. Ascenso, N. Marques, Inorg. Chem., 2003, **42**, 7666-7673.

(29) W. J. Evans, D. K. Drummond, J. Am. Chem. Soc., 1989, **111**, 3329-3335.

(30) M. Schultz, J. M. Boncella, D. J. Berg, T. D. Tilley, R. A. Andersen, Organometallics, 2001, **21**, 460-472.

(31) S. J. Kraft, P. E. Fanwick, S. C. Bart, Inorg. Chem., 2010, **49**, 1103-1110.

(32) K. Kalyanasundaram, Coord. Chem. Rev., 1982, **46**, 159-244.

(33) A. Juris,V. Balzani, F. Barigelletti, S. Campagna, P. Belser, A. Von Zelewsky, Coord. Chem. Rev., 1988, **84**, 84-277.

(34) P. Renaud, M. P. Sibi, Eds., Radicals in Organic Synthesis, Wiley-VCH, Weinheim, Germany, 2001.

(35) D. A. Nicewicz, D. W. C. MacMillan, Science, 2008, **322**, 77-80.

(36) J. H. Penn, R. C. Plants, A. Liu, Chem. Commun., 1999, 2359-2360.

(37) G. Nord, O. Wernberg, J. Chem. Soc., Dalton Trans., 1972, 866-868.

(38) G. Nord, O. Wernberg, J. Chem. Soc., Dalton Trans., 1975, 845-849.

(39) M. Kimura, G. G. Wada, Inorg. Chem., 1978, **17**, 2239-2242.

(40) J. Grodkowski, P. Neta, C. J. Schlesener, J. K. Kochi, J. Phys.Chem., 1985, **89**, 4373-4378.

(41) R. Schmid, K. Kirchner, F. L. Dickert, Inorg. Chem., 1988, **27**, 1530-1536.

(42) T. S. Lee, I. M. Kolthoff, D. L. Leussing, J. Am. Chem. Soc., 1948, **70**, 2348-2352.

(43) J. E. Dickens, F. Basolo, H. M. Neumann, J. Am. Chem. Soc., 1957, **79**, 1286-1290.

(44) D. W. Margerum, J. Am. Chem. Soc., 1957, **79**, 2728-2733.

(45) B. R. James, J. R. Lyons, R. J. P. Williams, Biochemistry, 1962, **1**, 379-385.

(46) G. Nord, B. Pedersen, E. Bjergbakke, J. Am. Chem. Soc., 1983, **105**, 1913-1919.

(47) J.-F. Capon, F. Gloaguen, P. Schollhammer, J. Talarmin, J. Electroanal. Chem., 2006, **595**, 47.

(48) G. A. N. Felton, A. K. Vannucci, J. Chen, L. T. Lockett, N. Okumura, B. J. Pedro, U. I. Zakai, D. H. Evans, R. S. Glass, D. L. Lichtenberger, J. Am. Chem. Soc., 2007, **129**, 12521-12530.

(49) J. Windhager, M. Rudolph, S. Bräutigam, H. Görls, W. Weigand, Eur. J. Inorg. Chem., 2007, 2748-2760.

(50) J.-F. Capon, S. Ezzaher, F. Gloaguen, F. Y. Pétillon, P. Schollhammer, J. Talarmin, T. Davin, J. E. McGrady, K. W. Muir, New J. Chem., 2007, **31**, 2052-2064.

(51) S. J. Borg, T. Behrsing, S. P. Best, M. Razavet, X. Liu, C. J. Pickett, J. Am. Chem. Soc., 2004, **126**, 16988-16999.

(52) S. J. Borg, M. I. Bondin, S. P. Best, M. Razavet, X. Liu, C. J. Pickett, Biochem. Soc. Trans., 2005, **33**, 3-6.

(53) I. Aguirre de Carcer, A. DiPasquale, A. L. Rheingold, D. M. Heinekey, Inorg. Chem., 2006, **45**, 8000-8002.

(54) S. J. Borg, J. W. Tye, M. B. Hall, S. P. Best, Inorg. Chem., 2007, **46**, 384-394.

(55) T. K. Mukhopadhyay, R. K. Feller, F. N. Rein, N. J. Henson, N. C. Smythe, J. C. Gordon, Chem. Commun., 2012, **48**, 8670-8672.

(56) C. C. Scarborough, K. Wieghardt, Inorg. Chem., 2011, **50**, 9773-9793.

(57) F. I. Adam, G. Hogarth, S. E. Kabir, I. Richards, C.R. Chim., 2008, **11**, 890-905.

(58) S. Ezzaher, J.-F. Capon, F. Gloaguen, F. Y. Pétillon, P. Schollhammer, J. Talarmin, Inorg. Chem., 2007, **46**, 3426-3428.

(59) A. K Justice, G. Zampella, L. De Gioia, T. B. Rauchfuss, J. I. van der Vlugt, S. R. Wilson, Inorg. Chem., 2007, **46**, 1655-1664.

(60) S. Ezzaher, A. Gogoll, C. Bruhn, S. Ott, Chem. Commun., 2010, **46**, 5775-5777.

(61) W. Dong, M. Wang, X. Liu, K. Jin, G. Li, F. Wang, L. Sun, Chem. Commun., 2006, 305-307.

(62) K. Izutsu, in Acid-Base Dissociation Constants in Dipolar Aprotic Solvents, Blackwell Scientific Publications, Oxford, 1990.

(63) A. Winter, L. Zsolnai, G. Huttner, Z. Naturforsch., 1982, **37b**, 1430-1436.

(64) SMART Version 5.628; Bruker AXS, Inc., 5465 East Cheryl Parkway, Madison, WI 53711-5373, 2003.

(65) SAINT Version 6.36A; Bruker AXS, Inc., 5465 East Cheryl Parkway, Madison, WI 53711-5373, 2002.

(66) G. M. Sheldrick, SADABS Version 2.10; University of Göttingen, Göttingen, Germany, 2003.

(67) G. M. Sheldrick, A short history of SHELX. Acta Crystallogr., 2008, **A64**, 112-122.

(68) M. J. Frisch, G. W. Trucks, H. B. Schlegel, G. E. Scuseria, M. A. Robb, J. R. Cheeseman, G. Scalmani, V. Barone, B. Mennucci, G. A. Petersson, H. Nakatsuji, M. Caricato, X. Li, H. P. Hratchian, A. F. Izmaylov, J. Bloino, G. Zheng, J. L. Sonnenberg, M. Hada, M. Ehara, K. Toyota, R. Fukuda, J. Hasegawa, M. Ishida, T. Nakajima, Y. Honda, O. Kitao, H. Nakai, T. Vreven, J. A. Montgomery Jr., J. E. Peralta, F. Ogliaro, M. Bearpark, J. J. Heyd, E. Brothers, K. N. Kudin, V. N. Staroverov, R. Kobayashi, J. Normand, K. Raghavachari, A. Rendell, J. C. Burant, S. S. Iyengar, J. Tomasi, M. Cossi, N. Rega, J. M. Millam, M. Klene, J. E. Knox, J. B. Cross, V. Bakken, C. Adamo, J. Jaramillo, R. Gomperts, R. E. Stratmann, O. Yazyev, A. J. Austin, R. Cammi, C. Pomelli, J. W. Ochterski, R. L. Martin, K. Morokuma, V. G. Zakrzewski, G. A. Voth, P. Salvador, J. J. Dannenberg, S. Dapprich, A. D. Daniels, O. Farkas, J. B. Foresman, J. V. Ortiz, J. Cioslowski, D. J. Fox, GAUSSIAN 09 (Revision A.02), Gaussian, Inc., Wallingford, CT, 2009.

(69) A. D. Becke, J. Chem. Phys., 1993, **98**, 5648-5652.

(70) C. Lee, W. Yang, R. G. Parr, Phys. Rev. B: Condens. Matter, 1988, **37**, 785-789.

(71) A. E. Reed, L. A. Curtiss, F. Weinhold, Chem. Rev., 1988, **88**, 899-926.

(72) K. B. Wiberg, Tetrahedron, 1968, **24**, 1083-1096.

(73) JIMP2, version 0.091, a free program for the visualization and manipulation of molecules: M. B. Hall, R. F. Fenske, Inorg. Chem., 1972, **11**, 768-775.

(74) J. Manson, C. E. Webster and M. B. Hall, Texas A&M University, College Station, TX, 2006, http://www.chem.tamu.edu/jimp2/index.html.